Influence of metal-molecule contacts on decay coefficients and specific contact resistances in molecular junctions

Gunuk Wang,[1] Tae-Wook Kim,[1] Hyoyoung Lee,[2] and Takhee Lee[1,*]

[1]*Department of Materials Science and Engineering, Gwangju Institute of Science and Technology, Gwangju 500-712, Korea*
[2]*National Creative Research Initiatives, Center for Smart Molecular Memory, IT Convergence Components Laboratory,*
Electronics and Telecommunication Research Institute, Daejeon 305-350, Korea

The effect of metal-molecule contacts in molecular junctions is studied based on the analysis of a statistically significant number of devices and a proposed multibarrier tunneling (MBT) model, where a metal-molecule-metal junction is divided into three individual barriers: a molecular-chain body and metal-molecule contacts on either side of molecule. Using the MBT model with the statistical analysis, we could derive and distinguish decay coefficients for contact barriers (β_1, β_2), contact-dependent and contact-independent decay coefficients (β_0 vs β_{body}), and specific contact resistances in terms of different molecular length and different natures of metal-molecule contacts.

I. INTRODUCTION

Molecular electronics utilizing functional molecules as the ultimate nanoscale electronic components have demonstrated their potential in device applications in a variety of functional electronic device components for ultrahigh density future electronics.[1–7] However, despite the numerous potential advantages of molecular electronics as compared to traditional silicon-based electronics, there are many issues and challenges that need to be overcome to apply molecules to actual electronic circuits. Among those, metal-molecule contact is important not only for understanding the transport properties of molecular devices[8–14] but also for realizing reproducible molecular electronic devices, due to its role in controlling metal-molecule interfaces.[12–16]

Here, we report the influence of metal-molecule contacts in molecular junctions and the essential charge transport mechanisms using a proposed multibarrier tunneling (MBT) model where the metal-molecule-metal junction can be divided into three parts: the molecular-chain body with metal-molecule contacts on either side of molecule. The MBT model in our study will help introduce an insight for studying charge transport mechanisms, focused on the metal-molecule contacts in molecular electronic devices or other nanoscale devices.

II. EXPERIMENT

A. Device fabrication

As shown in Fig. 1, molecular devices were fabricated as vertical metal-molecule-metal (MMM) structures with microscale via-hole junctions (diameter of ~ 2 μm) where molecular monolayers were sandwiched between the top and bottom Au electrodes. First, a conventional optical lithography method was used to pattern the bottom electrodes made with Au (1000 Å)/Ti (50 Å) on a p-type (100) Si substrate covered with thermally grown 3000 Å thick SiO_2 by an electron beam evaporator, under a pressure of $\sim 10^{-7}$ Torr and a deposition rate of 0.1 Å/s. The patterned bottom electrodes were deposited by a SiO_2 layer (700 Å thick) using plasma enhanced chemical vapor deposition. Then, to expose Au surfaces, reactive ion etching (RIE) was performed to make a circular hole with 2 μm diameter through the SiO_2 layer. The alkyl self-assembled monolayers were formed on the exposed Au surfaces, and a thermal evaporator was used to complete the MMM junction on the top Au electrode. The evaporation was done with a shadow mask on the chips, with a liquid nitrogen cooled stage to avoid thermal damage to the active molecular component, under a pressure of $\sim 10^{-6}$ Torr. For the same reason, the deposition rate of the
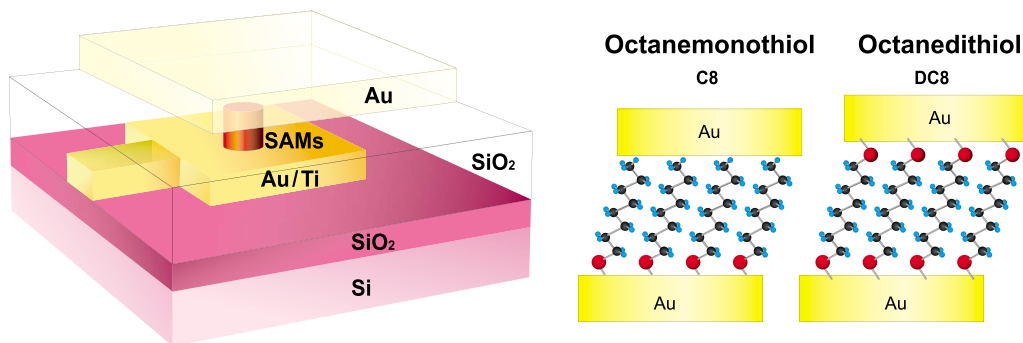
FIG. 1. (Color online) Schematics of vertical MMM structures (left) with microscale via-hole junctions used in this study and the configurations of C8 (middle) and DC8 (right) MMM junctions.
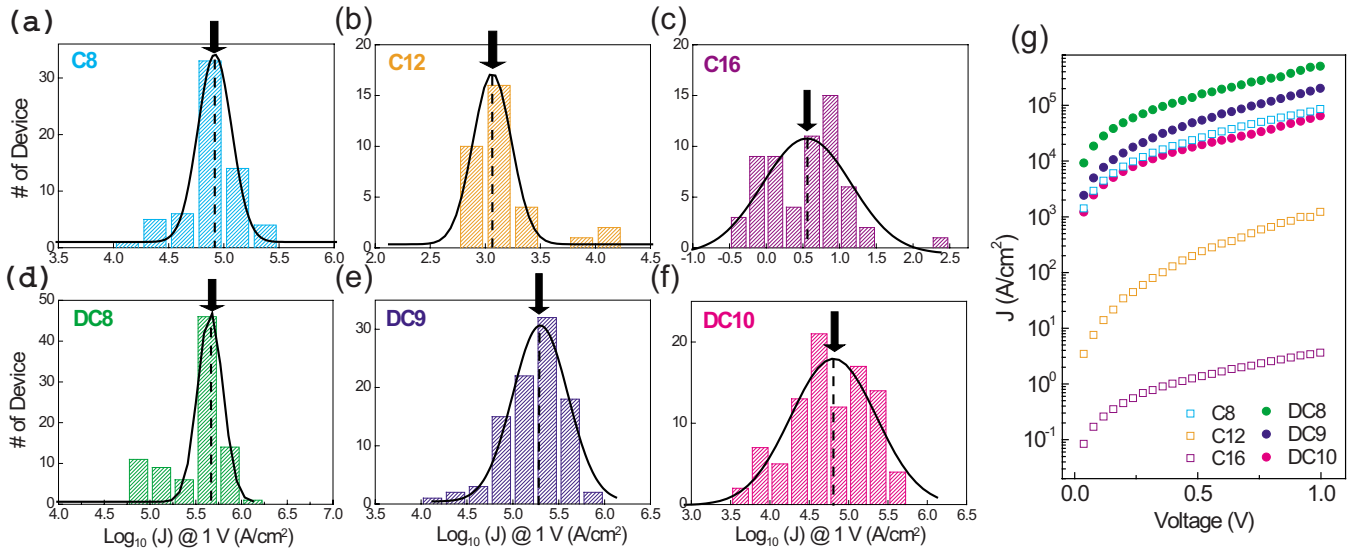
FIG. 2. (Color online) The statistical histograms of log(J) measured at 1.0 V for (a) C8, (b) C12, (c) C16, (d) DC8, (e) DC9, and (f) DC10. The line curves are fitting results obtained from the histograms with Gaussian functions and the mean positions are indicated with arrows. (g) Current density-voltage characteristics of representative devices chosen from the mean positions of the fitted Gaussian functions.

top Au electrode was kept very low, typically at ~0.1 Å/s with a total Au thickness of ~500 Å. Room temperature current-voltage characteristics of as-fabricated molecular devices were carried out using a semiconductor parameter analyzer (HP4155A).

B. Formation of self-assembled monolayers

For our experiments, six different ~5 mM alkanethiol solutions were prepared by adding ~10 μl alkanethiol to ~10 ml anhydrous ethanol (Aldrich Chem. Co). The samples were left in the solution for 24–48 h to allow a self-assembled monolayer to assemble on the Au surfaces exposed by RIE in a nitrogen-filled glove box with oxygen of less than ~10 ppm. Alkanemonothiols (Aldrich Chem. Co) and alkanedithiols (Aldrich Chem. Co and Tokyo Chem. Industry) of different molecular lengths, octanemonothiol [$CH_3(CH_2)_7SH$, C8], dodecanemonothiol [$CH_3(CH_2)_{11}SH$, C12], hexadecanemonothiol [$CH_3(CH_2)_{15}SH$, C16], octanedithiol [$HS(CH_2)_8SH$, DC8], nonanedithiol [$HS(CH_2)_9SH$, DC9], and decanedithol [$HS(CH_2)_{10}SH$, DC10], were used to form the active molecular components

in MMM devices. As an example, the configurations of C8 and DC8 MMM junctions are schematically illustrated in Fig. 1 (right side).

III. RESULTS

A. Statistical analysis of electronic characteristics

We fabricated and characterized a significantly large number of such molecular devices (27 840 devices in total) to statistically analyze the molecular electronic properties of a sufficient number of "working" molecular electronic devices (427 devices). The working devices displaying molecular properties were determined based on the statistical distribution of the current densities of the fabricated devices. Basically, working molecular electronic devices were extracted from devices showing a majority of current densities in the statistical distribution, by using a Gaussian function [Figs. 2(a)–2(f)]. The detailed criterion for determining working devices has been reported elsewhere.[17] As summarized in Table I, the numbers of C8, C12, C16, DC8, DC9, and DC10 working devices were 63, 33, 60, 84, 94, and 93, respec-

TABLE I. Summary of results for the fabricated devices [note: working and nonworking devices were defined by statistical analysis with Gaussian fitting on histogram of the logarithmic scale current densities (Ref. 17)].

	No. of fabricated devices	Fab. failure	Short	Open	Nonworking	Working			Device yield
						C8	C12	C16	
Monothiol	13440 (100%)	392 (2.9%)	11744 (87.4%)	1103 (8.2%)	45 (0.3%)	63 (1.41%)	33 (0.69%)	60 (1.44%)	156 (1.2%)
						DC8	DC9	DC10	
Dithiol	14400 (100%)	472 (3.28%)	12340 (85.7%)	1252 (8.69%)	65 (0.45%)	84 (1.75%)	94 (1.96%)	93 (1.94%)	271 (1.9%)

tively, among the total 27 840 fabricated devices. Then, the device yields were found as ~1.2% (156/13 440) for monothiol and ~1.9% (271/14 440) for dithiol devices. Since the device yield (~1.75%) of DC8 dithiol devices is not much different from that of C8 monothiol devices (~1.41%), this result may suggest that device yield is not much affected by the metal-molecule contact but rather affected more by the device structures, fabrication condition, and quality of the self-assembled monolayers. In this study, the use of a statistical approach is very significant, as the analysis of a large number of devices increases the ability to develop more accurate and meaningful characteristics of molecular systems.[17–19] Note that the main conduction through alkyl molecular devices is the tunneling mechanism, which can be checked by temperature-independent current-voltage characteristics.[20,21] In our study, a few selected devices indeed exhibited a tunneling conduction mechanism (data not shown here).

Figures 2(a)–2(f) present the statistical histograms of current densities in logarithmic scale for different lengths of alkanemonothiols (C8, C12, and C16) and alkanedithiols (DC8, DC9, and DC10) at 1.0 V with the mean positions as representative devices indicated with arrows from the fitting results by Gaussian functions. The current densities for these representative devices were found to be ~8.3×10^4, 1.2×10^3, 3.5, 4.9×10^5, 2.0×10^5, and 6.3×10^4 A/cm² at 1.0 V for C8, C12, C16, DC8, DC9, and DC10, respectively. The current density-voltage (J-V) characteristics for these six representative devices are plotted in Fig. 2(g). The conductance and J-V characteristics are clearly dependent on the molecular length and metal-molecular contacts (i.e., monothiol vs dithiol). This observation is supported by previous reports of MMM junctions that have shown that the current density for alkanedithiol is higher than that for alkanemonothiol due to their different natures of metal-molecule contact properties (chemisorbed vs physisorbed contact) at Au-molecule contacts.[11,22] The histograms in Figs. 2(a)–2(f) show the distribution of the logarithmic current densities, indicating the existence of fluctuation factors causing the exponential distribution in the current densities.[17] The variation of junction area may exist, but the area fluctuation does not produce an exponential distribution in current; instead, fluctuation in the tunneling path is probably responsible for the distribution data of Figs. 2(a)–2(f). Some fluctuations in molecular configurations in the self-assembled monolayers in the device junctions are possible, such as fluctuations in molecular configuration or microstructures in metal-molecule contacts.[23,24]

B. Multibarrier tunneling model through alkanethiol molecular junction

To investigate the effect of metal-molecule contacts on the electronic transport, we propose a MBT model, which generalizes the Simmons tunneling model, a widely used model for describing a rectangular tunneling barrier.[25] As compared to the Simmons tunneling model where the tunneling barrier is represented by a single barrier, the MMM junction in the MBT model can be divided into three parts: a

molecular-chain body and metal-molecule contacts on either side of molecule, represented as three individual conduction barriers, as schematically illustrated in Fig. 3(a). In the n-alkanedithiol MMM junction, there is one molecular-chain body barrier [$(CH_2)_n$] (n is the number of carbon units) and two chemisorbed contact barriers [Au-S-C] on either side. Conversely, the n-alkanemonothiol MMM junction with the same molecular-chain body barrier [$(CH_2)_n$] as the n-alkanedithiol junction has one chemisorbed contact barrier [Au-S-C] and one physisorbed contact barrier [CH_3/Au]. This approach of separation of the metal-molecule contact and the molecular body from alkanethiol MMM junction is reasonable since hybridization of the metal-molecule wave function decays rapidly into the junction for alkanethiol devices.[12,13]

In Fig. 3(a), the widths of the barriers for d_1, d_{body}, and d_2 represent the length of the chemisorbed contact on the molecule [Au-S-C], a molecular-chain body region [$(CH_2)_n$], and the physisorbed contact on the molecule [CH_3/Au], respectively. Here, d_1 ([Au-S-C]) is ~3.80 Å and d_2 ([CH_3/Au]) is ~2 Å.[26] d_{body} is the projected length along the molecular chain and the incremental length per carbon atom (Δd_{body} [CH_2]) is ~1.25 Å; all of which were obtained using the CHEM3D software following the method in previous literature.[26] The length d_{body} is identical for n-alkanemonothiol and n-alkanedithiol with the same n value; for example, octanemonothiol (C8) and octanedithiol (DC8) have an identical length, d_{body} [$(CH_2)_8$, ~7.46 Å]. The total width of the barriers in alkanemonothiol (alkanedithiol) is $d = d_1 + d_{body} + d_2(d_1)$.

For small length molecules with a large highest occupied molecular orbital lowest unoccupied molecular orbital energy gap, such as alkyl chain molecules, coherent tunneling is the main conduction mechanism of the electronic charge transport at a relatively low bias regime.[16,27,28] In the low bias regime, the tunneling current density can be approximated as[11,16,25,27]

$$J \approx \frac{(2m\Phi_B)^{1/2}e^2\alpha}{4\pi^2\hbar^2 d}V\exp\left[-\frac{2(2m)^{1/2}}{\hbar}\alpha(\Phi_B)^{1/2}d\right], \quad (1)$$

$$\beta_0 = \frac{2(2m)^{1/2}}{\hbar}\alpha(\Phi_B)^{1/2}, \quad (2)$$

where m is the electron mass, d is the total barrier width or molecular length, Φ_B is the rectangular barrier height at zero bias, e is the electronic charge, V is the applied bias, and α is a unitless adjustable parameter introduced to modify the simple rectangular barrier model, or to account for the effective mass of the tunneling electrons through a rectangular barrier. β_0 is the decay coefficient in a low bias regime, which reflects the degree of decrease in wave function of the tunneling electron through the molecular tunnel barrier. A higher decay coefficient implies a faster decay of the wave function, i.e., lower electron tunneling efficiency.

In the MBT model, it is possible to describe the overall slope of wave function decay through the barriers based on the magnitude of the β_0 value, and this overall decay can be further decomposed to three individual decays through three
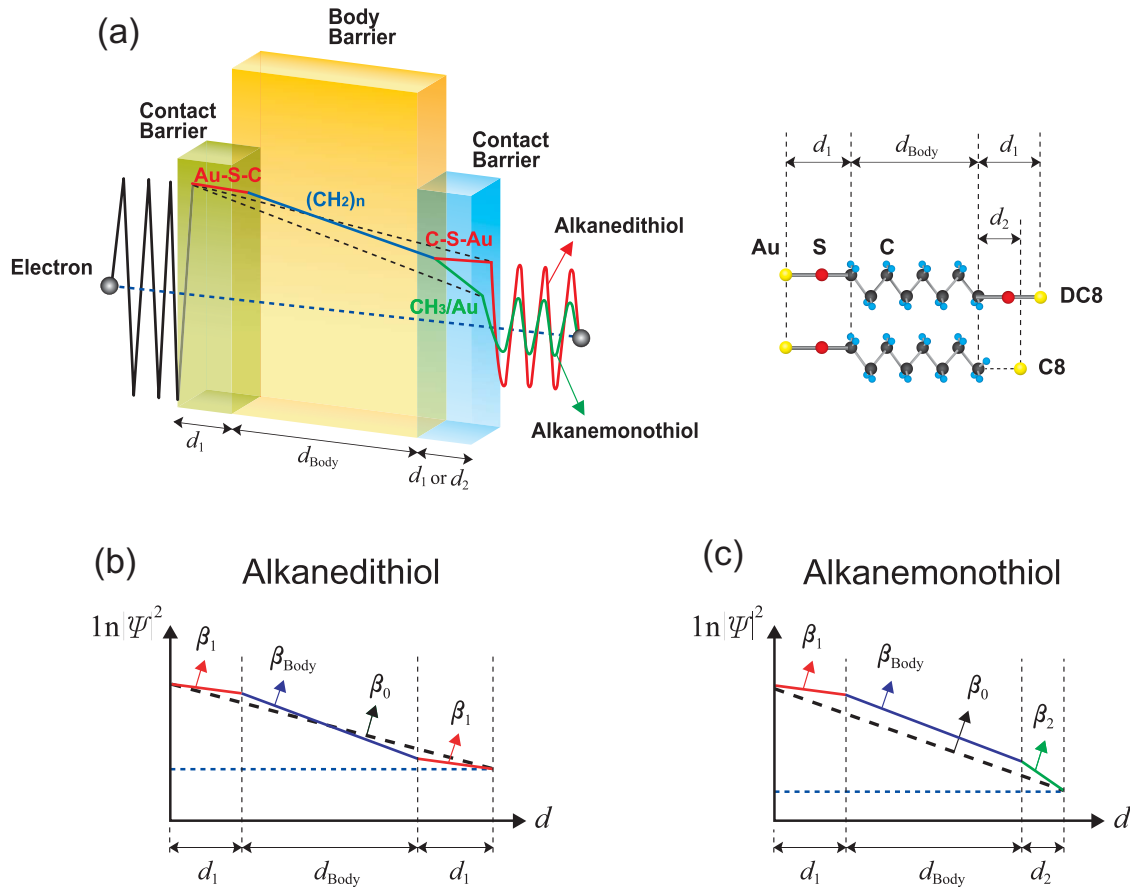
FIG. 3. (Color online) (a) Left is an illustration of the MBT model. Right is a schematic of barrier widths for C8 and DC8. Schematics of MBT model (b) for an alkanedithiol MMM junction and (c) for an alkanemonothiol MMM junction.

individual barriers, as shown in Fig. 3. The β_0 can be expressed as Eq. (3) for alkanemonothiol (alkanedithiol) junctions from the consideration of geometric configurations,

$$\beta_0 = \frac{\beta_1 d_1 + \beta_{\text{body}} d_{\text{body}} + \beta_{1(2)} d_{1(2)}}{d_1 + d_{\text{body}} + d_{1(2)}}. \quad (3)$$

One can see that β_0 converges to β_{body} for a very long molecule. Also, $\alpha(\Phi_B)^{1/2}$ can be expressed as Eq. (4) by combining Eqs. (2) and (3),

$$\alpha(\Phi_B)^{1/2} = \frac{\hbar}{2(2m)^{1/2}} \frac{\beta_1 d_1 + \beta_{\text{body}} d_{\text{body}} + \beta_{1(2)} d_{1(2)}}{d_1 + d_{\text{body}} + d_{1(2)}}. \quad (4)$$

As mentioned above, because the main conduction mechanism is coherent (elastic) tunneling at the low bias regime (and at room temperature), it is assumed that the energy of electron tunneling through the molecular barriers does not decrease, as expressed by the horizontal blue dashed line in Fig. 3(a). Furthermore, due to the different natures of the metal-molecule contact properties, electron transmission for the chemisorbed contact [Au-S-C] is found to be more efficient than that for the physisorbed contact [CH_3/Au]. As a result, the slope (β_0) for alkanemonothiol junctions is steeper than that for alkanedithiol junctions, as illustrated by the black dashed lines in Fig. 3. In this MBT model, it was possible to define β_1 (β_2) as the components of the decay

coefficients corresponding to the chemisorbed (physisorbed) contact barrier width d_1 (d_2), as expressed by the red (green) solid lines in Fig. 3. Similarly, β_{body} is the decay coefficient component for the molecular-chain body barrier (blue solid lines).

Figure 4(a) shows the statistical distribution of β_0 values obtained for different length alkanemonothiol and alkanedithiol MMM devices. In this plot, β_0 values were determined from fitting the *I-V* data of all the "statistically defined working" molecular electronic devices (total 427 devices) with the Simmons tunneling model. The values for the mean and standard deviation of β_0 are presented as 0.81 ± 0.05, 0.83 ± 0.03, and 0.87 ± 0.05 Å^{-1} for C8, C12, and C16 alkanemonothiols and 0.55 ± 0.06, 0.57 ± 0.06, and 0.58 ± 0.08 Å^{-1} for DC8, DC9, and DC10 alkanedithiols, respectively. As previously mentioned, the β_0 values for alkanemonothiol devices appear to be larger than those for alkanedithiol devices due to the poor tunneling rate of physisorbed contact [CH_3/Au] in alkanemonothiol junctions, as compared to alkanedithiol junctions. Also, a slight increase of β_0 values in Figs. 4(a) and 4(b) can be seen as the molecular length increases, which reflects the different tunneling rates for different lengths of alkanethiols, i.e., the wave function of the tunneling electron decays further when it tunnels through longer molecules. The solid lines in Fig. 4(b) are the results calculated using the estimated β_{body}, β_1, and β_2 values determined from the MBT model (Table II). More-
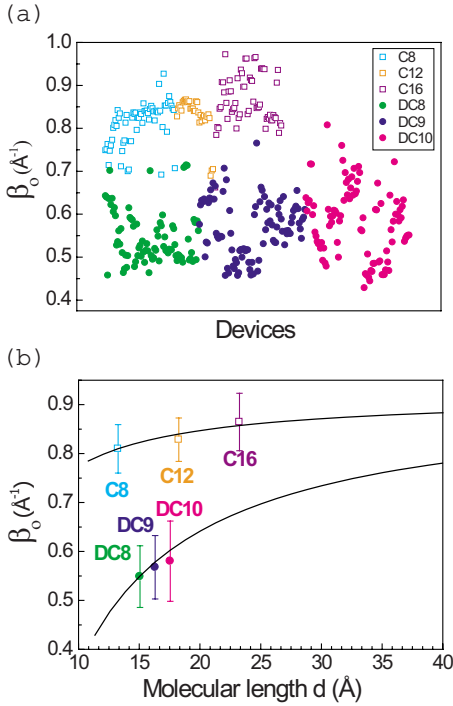
FIG. 4. (Color online) The overall decay coefficient β_0 for different length alkanemonothiol (C8, C12, and C16) and alkanedithiol (DC8, DC9, and DC10) junctions. (b) The mean (symbols) and standard deviations (error bars) of β_0 vs molecular length d. The black solid lines were calculated from the MBT model.

over, Fig. 4(b) shows that the difference in β_0 values between monothiol and dithiol becomes larger as the molecular length decreases. This phenomenon explains that the metal-molecular contact effect becomes relatively more important than the molecular-chain body effect in electronic transport for shorter molecules. On the contrary, if the molecular length increases, the molecular-chain body effect becomes more important and the β_0 values of monothiol and dithiol molecular systems become closer and eventually converge to the body decay coefficient (β_{body}), as seen in Fig. 4(b).

At low bias, Eqs. (1) and (3) can be used to determine the resistance R of the Ohmic regime as

$$R = \frac{4\pi^2\hbar^2}{A(2m)^{1/2}e^2}\left[\frac{d_1 + d_{body} + d_{1(2)}}{(\Phi_B)^{1/2}\alpha}\right]\exp[\beta_1 d_1 + \beta_{body}d_{body} + \beta_{1(2)}d_{1(2)}],$$

(5)

FIG. 5. (Color online) Semilogarithmic plot of the resistance R vs the molecular-chain body length d_{body} for alkanemonothiol and alkanedithiol junctions. The solid lines are exponential fitting results, giving the molecular-chain body decay coefficient β_{body}.

where R_0 is the contact resistance that can be defined in the limiting case when d_{body} approaches zero and expressed as Eq. (6) for alkanemonothiol and alkanedithiol,

$$R_0 = \frac{8\pi^2\hbar}{Ae^2}\left[\frac{(d_1 + d_{1(2)})^2}{\beta_1 d_1 + \beta_{1(2)}d_{1(2)}}\right]\exp[\beta_1 d_1 + \beta_{1(2)}d_{1(2)}].$$

(6)

Unlike the β_0 value that describes the overall decay coefficient, the β_{body} value is the decay coefficient component only for the molecular-chain body barrier. The molecular-chain body decay coefficient $\beta_{body} = \Delta\ln R / \Delta d_{body}$ can be determined from the slopes in the semilogarithmic plot of resistance R vs the molecular-chain body length d_{body}, as shown in Fig. 5. Here, R is the resistance in the low bias regime obtained from the linear fit of low bias I-V data ($0 < V < 0.3$ V) for each device. From the slopes in Fig. 5, the β_{body} values were determined to be $\sim 0.93 \pm 0.03$ and $\sim 0.92 \pm 0.08$ Å^{-1} for alkanemonothiol and alkanedithiol, respectively, almost identical values for the two molecular systems. Thus, one should note that the β_{body} value is the molecular length-independent decay coefficient that is dependent on the molecular structure but not on metal-molecule contacts, whereas the β_0 value is the molecular length-dependent overall decay coefficient that depends not only on the molecular structures but also on the form of the metal-molecule contact (i.e., chemisorbed or physisorbed). The β_1, β_2, and β_0 for the alkyl MMM junctions can be calculated from the observed $\beta_{body} \sim 0.92$ Å^{-1}, β_0 values for

TABLE II. A summary of the experimental and calculated values for decay coefficients, contact resistances, and specific contact resistances.

		β_{body} (Å^{-1})	β_1 (Å^{-1})	β_2 (Å^{-1})	R_o (Ω)	R_c (Ω cm^2)
Alkanemonothiol	Calc. value	0.92	0.19	1.58	0.43	1.36×10^{-8}
	Expt. value	0.93 ± 0.03			0.72 ± 0.58	$(2.27 \pm 1.83) \times 10^{-8}$
Alkanedithiol	Calc. value	0.92	0.19		0.17	5.46×10^{-9}
	Expt. value	0.92 ± 0.08			0.17 ± 0.08	$(5.40 \pm 2.48) \times 10^{-9}$
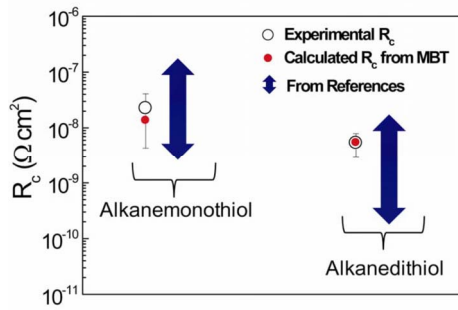
FIG. 6. (Color online) Experimental and calculated specific contact resistance R_c. The blue arrows represent the range of the estimated R_c values from the contact resistances reported in literature (Refs. 11, 26, 29, and 30).

C8 and DC8, and the widths of barriers (d_1, d_{body}, and d_2).

The contact resistance (R_0) can be considered a method of investigating the metal-molecule contacts.[11,26,29,30] However, since R_0 depends on the junction area, the specific contact resistance (R_c), the junction area compensated quantity, is generally obtained and compared among devices with different junction areas. Figure 6 presents the experimental and theoretical values for R_c for our alkanemonothiol and alkanedithiol devices at a low bias regime. Here, the specific contact resistance R_c ($=R_0A$) can be obtained by multiplying the contact resistance (R_0) with the contact junction area (A) ($\sim 3.14 \times 10^{-8}$ cm^2 for our molecular devices). The contact resistance (R_0) was found by extrapolating the observed resistance (Fig. 5) to a zero molecular-chain body length ($\sim 0.72 \pm 0.58$ Ω for alkanemonothiol and $\sim 0.17 \pm 0.08$ Ω for alkanedithiol). Then, R_c was calculated as ($\sim 2.27 \pm 1.83$) $\times 10^{-8}$ Ω cm^2 for alkanemonothiol and ($\sim 5.40 \pm 2.48$) $\times 10^{-9}$ Ω cm^2 for alkanedithiol. Using the MBT model, R_c could also be estimated as $\sim 1.36 \times 10^{-8}$ Ω cm^2 for al-

kanemonothiol and $\sim 5.46 \times 10^{-9}$ Ω cm^2 for alkanedithiol, both of which are in good agreement with the experimental values we obtained. Table II summarizes the experimental and calculated quantities of decay coefficients and contact and specific contact resistances for our measurements.

Note that our analysis with the MBT model does not consider the details of the Fermi level alignment and molecular binding sites, which will generally influence the charge transport of molecular devices.[31] Furthermore, the transport property values obtained from our experimental results with microscale molecular junctions are an ensemble average effect with various microstructures of metal-molecule contacts and binding sites and thus should not be compared with single-molecular measurement results,[13] due to the contribution from the probability amplitude of multiple reflection and the possibility of cooperative effects between individual molecules in the ensemble of molecules.

IV. CONCLUSION

In summary, we studied the effect of metal-molecule contacts in MMM junctions with a multibarrier tunneling model, based on the statistical analysis of a large number of devices. We obtained the transport parameters such as individual decay coefficients (β_1, β_2, β_0, β_{body}) and specific contact resistances with different molecular lengths and different natures of contact properties.

ACKNOWLEDGMENTS

*tlee@gist.ac.kr

[1] *Molecular Nanoelectronics*, edited by M. A. Reed and T. Lee (American Scientific, Stevenson Ranch, 2003).

[2] A. Nitzan and M. A. Ratner, Science **300**, 1384 (2003).

[3] J. Park, A. N. Pasupathy, J. I. Goldsmith, C. Chang, Y. Yaish, J. R. Petta, M. Rinkoski, J. P. Sethna, H. D. Abruña, P. L. McEuen, and D. C. Ralph, Nature (London) **417**, 722 (2002).

[4] J. Chen, M. A. Reed, A. M. Rawlett, and J. M. Tour, Science **286**, 1550 (1999).

[5] C. P. Collier, E. W. Wong, M. Belohradský, F. M. Raymo, J. F. Stoddart, P. J. Kuekes, R. S. Williams, and J. R. Heath, Science **285**, 391 (1999).

[6] Y. Chen, G. Y. Jung, D. A. A. Ohlberg, X. Li, D. R. Stewart, J. O. Jeppesen, K. A. Nielsen, J. F. Stoddart, and R. S. Williams, Nanotechnology **14**, 462 (2003).

[7] J. E. Green, J. W. Choi, A. Boukai, Y. Bunimovich, E. Johnston-Halperin, E. DeIonno, Y. Luo, B. A. Sheriff, K. Xu, Y. S. Shin, H.-R. Tseng, J. F. Stoddart, and J. R. Heath, Nature (London) **445**, 414 (2007).

[8] S. Datta, W. Tian, S. Hong, R. Reifenberger, J. I. Henderson, and C. P. Kubiak, Phys. Rev. Lett. **79**, 2530 (1997).

[9] J. G. Kushmerick, D. B. Holt, J. C. Yang, J. Naciri, M. H. Moore, and R. Shashidhar, Phys. Rev. Lett. **89**, 086802 (2002).

[10] J. Taylor, M. Brandbyge, and K. Stokbro, Phys. Rev. Lett. **89**, 138301 (2002).

[11] V. B. Engelkes, J. M. Beebe, and C. D. Frisbie, J. Am. Chem. Soc. **126**, 14287 (2004).

[12] J. G. Kushmerick, Mater. Today **8**, 26 (2005).

[13] A. Salomon, D. Cahen, S. Lindsay, J. Tomfohr, V. B. Engelkes, and C. D. Frisbie, Adv. Mater. (Weinheim, Ger.) **15**, 1881 (2003).

[14] A. Salomon, T. Böcking, J. J. Gooding, and D. Cahen, Nano Lett. **6**, 2873 (2006).

[15] B. Xu and N. J. Tao, Science **301**, 1221 (2003).

[16] T. Lee, W. Wang, J. F. Klemic, J. J. Zhang, J. Su, and M. A. Reed, J. Phys. Chem. B **108**, 8742 (2004).

[17] T.-W. Kim, G. Wang, H. Lee, and T. Lee, Nanotechnology **18**, 315204 (2007).

[18] M. T. González, S. Wu, R. Huber, S. J. Molen, C. Schönenberger, and M. Calame, Nano Lett. **6**, 2238 (2006).

[19] S.-Y. Jang, P. Reddy, A. Majumdar, and R. A. Segalman, Nano Lett. **6**, 2362 (2006).

[20] W. Wang, T. Lee, and M. A. Reed, Phys. Rev. B **68**, 035416 (2003).

[21] N. B. Zhitenev, A. Erbe, and Z. Bao, Phys. Rev. Lett. **92**, 186805 (2004).

[22] X. D. Cui, A. Primak, X. Zarate, J. Tomfohr, O. F. Sankey, A. L. Moore, T. A. Moore, D. Gust, G. Harris, and S. M. Lindsay, Science **294**, 571 (2001).

[23] E. Lörtscher, H. B. Weber, and H. Riel, Phys. Rev. Lett. **98**, 176807 (2007).

[24] Y. Hu, Y. Zhu, H. Gao, and H. Guo, Phys. Rev. Lett. **95**, 156803 (2005).

[25] J. G. Simmons, J. Appl. Phys. **34**, 1793 (1963).

[26] D. J. Wold, R. Haag, M. A. Rampi, and C. D. Frisbie, J. Phys. Chem. B **106**, 2813 (2002).

[27] W. Wang, T. Lee, and M. A. Reed, Rep. Prog. Phys. **68**, 523 (2005).

[28] C. Joachim and M. Magoga, Chem. Phys. **281**, 347 (2002).

[29] C.-C. Kaun and H. Guo, Nano Lett. **3**, 1521 (2003).

[30] J. M. Beebe, V. B. Engelkes, L. L. Miller, and C. D. Frisbie, J. Am. Chem. Soc. **124**, 11268 (2002).

[31] S.-H. Ke, H. U. Baranger, and W. Yang, J. Am. Chem. Soc. **126**, 15897 (2004).